THE ARCHIVE OF MECHANICAL ENGINEERING

VOL. LVIII 2011 Number 2

10.2478/v10180-011-0010-x

Key words: modelling, diagnostics, axial piston pump, swash plate, signal analysis, vibration measurement

WALDEMAR ŁATAS [*], *JERZY STOJEK* [**]

DYNAMIC MODEL OF AXIAL PISTON SWASH-PLATE PUMP FOR DIAGNOSTICS OF WEAR IN ELEMENTS

The possibility of distinguishing and assessing the influences of defects in particular pump elements by registering vibration signals at characteristic points of the pump body would be a valuable way for obtaining diagnostic information. An effective tool facilitating this task could be a well designed and identified dynamic model of the pump. When applied for a specific type of the pump, such model could additionally help to improve its construction.

This paper presents model of axial piston positive displacement pump worked out by the authors After taking the simplifying assumptions and dividing the pump into three sets of elements, it was possible to build a discrete dynamic model with 13 degrees of freedom. According to the authors' intention, the developed dynamic model of the multi-piston pump should be used for damage simulation in its individual elements. By gradual change in values of selected construction parameters of the object (for example: stiffness coefficients, damping coefficients), it is possible to perform simulation of wear in the pump. Initial verification of performance of the created model was done to examine the effect of abrasive wear on the swash plate surface. The phase trajectory runs estimated at characteristics points of the pump body were used as a useful tool to determine wear of pump elements.

1. Introduction

Axial piston pumps take particularly important place in hydraulics systems. Moreover, correct functioning of the whole system depends on their proper operation.

Investigation on axial piston pumps is carried out worldwide in several research centres. The main topics are: the analysis of forces between the elements in relative motion [3, 5], the evaluation of flow inside the pump

[*] *Cracow University of Technology, Institute of Applied Mechanics, Al. Jana Pawła II 37, 31-864 Cracow, Poland*

[**] *AGH University of Science and Technology, Department of Process Control, al. Mickiewicza 30, 30-059 Cracow, Poland; e-mail: jerzy.stojek@autocom.pl*

[5], the reduction of noise and cavitations [8]. The purpose of this research was to create and analyse a dynamic model of axial piston swash-plate pump applicable for wear diagnostics of its elements.

The wear of particular pump elements most often leads to a decrease in the operational pump pressure and an increase in volumetric losses, thus in consequence it reduces the general pump efficiency and increases vibration and noise. The aim of vibration-acoustic exploitation diagnostics of pumps is to look for symptoms of hypothetical defects in the vibration signal. Mechanical complexity of the system and high level of disturbances cause that uncertainty of the diagnostics might be substantial. The possibility of distinguishing and assessing the influences of defects in particular pump elements by registering vibration signals at characteristic points of the pump body would be a valuable way for obtaining diagnostic information. An effective tool facilitating this task could be a well designed and identified dynamic model of the pump. When applied for a specific type of the pump, such model could additionally help to improve its construction.

2. Description of the modelled object

A positive-displacement pump is usually the basic element of drive systems and hydrostatic control units. The main task such a pump fulfils is to change mechanical input energy of a working medium into hydrostatic output energy in the pump's delivery pipe. In brief, the work of positive-displacement pump consists in forcing a defined volume of the working medium from the suction space into the pumping space (with leak-proof separation between these two spaces) by means of a system of displacement elements. The contemporary positive-displacement pumps can be divided into several categories, depending on the kind of motion which displacement elements make (for example, rotational pumps, piston pumps), depending on the efficiency of output flow (pumps with fixed and set efficiencies), and depending on the number of independent output flows (single flow and multi-flow pumps). The type of pumps, most frequently used in today's industry, are the axial piston pumps. This is because of many reasons, among which one can mention a wide range of individual efficiency for which such pumps are built (from 5 to 1000 [cm^3/turn]) as well as a high range of nominal exploitation pressures (45 [MPa] and more). This is also the reason why the authors decided to create a dynamic model of the structure of one of such positive-displacement pumps.

We choose a multi-piston axial swash-plate pump type WPTO2-10 [11], whose simplified diagram is shown in Fig. 1. In a pump of this type, the cylinder block (2) together with the system of pistons (3) is mounted coaxially

on the drive shaft (1). The shoes (4) of pistons slide on the surface of the immobile, inclined swash plate (5). The pistons rotate (together with the cylinder block) around the centreline of the shaft and make reciprocating motion in the cylinder holes, the results of which is pumping of the working medium. Additionally, the cylinder block slides on the immobile valve port plate (6) on which there are placed suction and pumping openings.

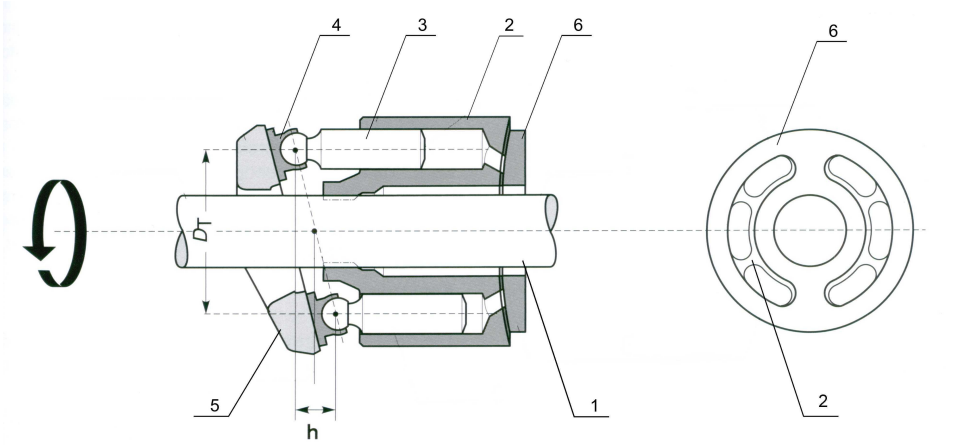

Fig. 1. General scheme of the axial multi-piston pump: 1 – shaft, 2 – cylinder block, 3 – piston, 4 – piston shoe, 5 – swash plate, 6 – valve port plate, D_T – cylinder port circle diameter, h – piston stroke [10]

In multi-piston pumps, the rotor system is usually the most important element which decides about the intensity of flow produced in the pump delivery pipe. The existing solutions of multi-piston pumps differ between one another according to the method of placing the rotor system in the pump construction, and according to the kind of its drive.

The basic rotor system in the investigated WPTO2-10 pump [11] consisted of a rotor composed of two elements (including the cylinder block) with seven pistons placed in the cylinder holes. The rotor system assembly was supported on a roller bearing (Fig. 2).

3. Formulating the dynamic model of the pump

Prior to creating the dynamic model of the WPTO2-10 axial piston pump, we took the following simplifying assumptions:

- the pump shell does not make rotational motion around Z axis;
- the angular velocity of the rotor is constant in the entire working cycle;

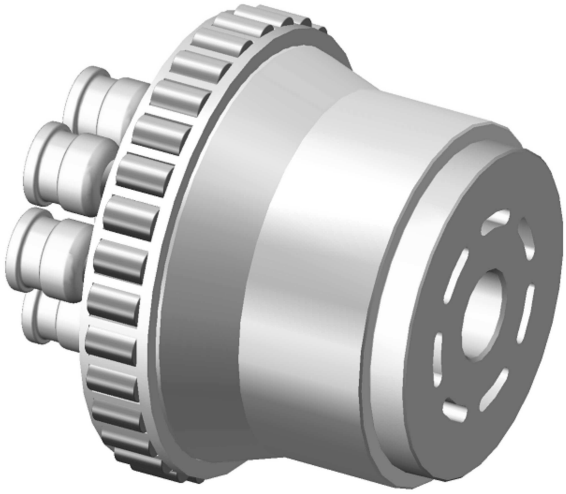

Fig. 2. Rotor system of the WPTO2-10 pump

- the pressures inside the suction and pumping ports are approximately constant, with pulsations resulting from sudden changes in the pressure at the cylinder hole caused by piston strokes;
- the pump is in the state of thermal balance, thus the oil viscosity does not change (physical properties of the oil are stable);
- the pressure course in the cylinder hole is a periodic function of the rotation angle of the rotor.

The construction diagram of the pump, adopted for developing the dynamic model, is presented in Fig. 3a. In the diagram, there are shown main elements of the pump together with their geometrical parameters. One can distinguish three sets of elements:

- the shell;
- the rotor;
- the separator.

The shell assembly consists of the casing, back and front closing lids, the swash plate, and the valve port plate. The rotor assembly consists of the drive shaft, the cylinder block with the set of pistons, and the set of three bearings. The separator assembly includes the retaining ring and the pressure spring. After taking the above assumptions and dividing the pump into three sets of elements, it was possible to build a discrete dynamic model with 13 degrees of freedom: 5 degrees for the shell assembly, 5 degrees for the rotor assembly, and 3 degrees for the separator assembly.

The subscripts used in descriptions refer to the following components:
F – shell, C – rotor, P – separator, T – piston, S – shoe.

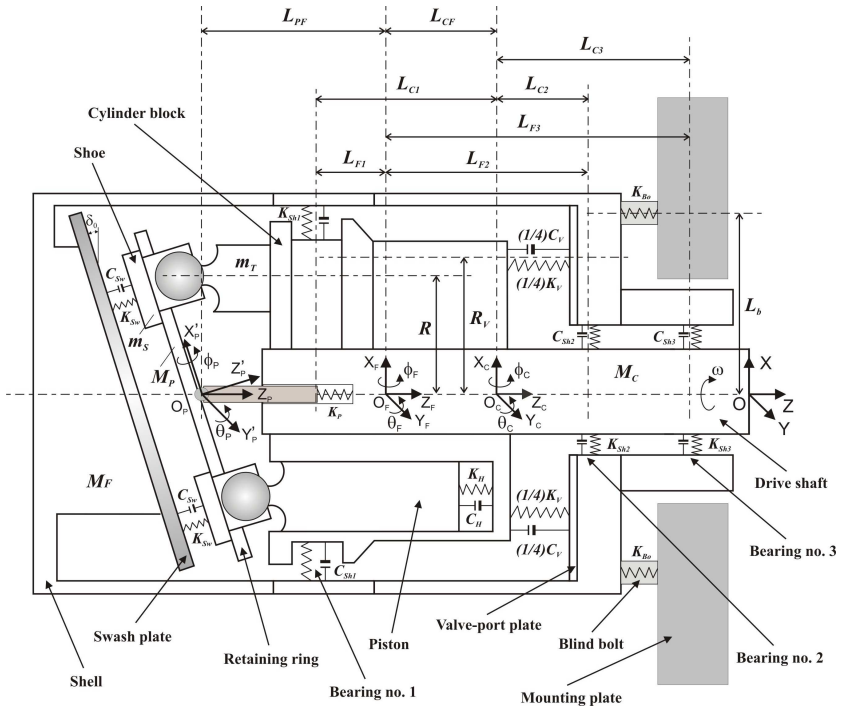

Fig. 3a Structural scheme of dynamic model of the axial piston-pump: O_P – mass centre of the retaining ring, O_C – mass centre of the cylinder block and drive shaft assembly, O_F – mass centre of the shell assembly

The symbols used in denotations are grouped and listed below:

$X_F, Y_F, Z_F, \varphi_F, \theta_F$ – linear displacements of mass centre of the shell assembly, and angular displacements around relevant axes (Fig. 3a);

$X_C, Y_C, Z_C, \varphi_C, \theta_C$ – linear displacements of mass centre of the cylinder block and drive shaft assembly, and angular displacements around relevant axes (Fig. 3a);

Z_P, φ_P, θ_P – linear displacement of mass centre of the retaining ring, and angular displacements around relevant axes (Fig. 3a);

M_F, I_{Fx}, I_{Fy} – mass and moments of inertia of the shell assembly;

$M_C, I_{Cx}, I_{Cy}, I_{Cz}$ – mass and moments of inertia of the cylinder block and drive shaft assembly;

$M_P, I_{Px'}, I_{Py'}, I_{Pz'}$ – mass and moments of inertia of the retaining ring;

m_S – mass of the piston shoe;

m_T, I_T – mass and moment of inertia of the piston (against the principal axis perpendicular to its centerline);

$K_{Box}, K_{Boy}, K_{Boz}$ – stiffness coefficients in X, Y and Z direction of the bolt between shell assembly and mounting plate;

C_{Sw}, K_{Sw} – damping and stiffness coefficients of the interface between piston shoe and swash plate;

$C^1_{Shx}, K^1_{Shx}, C^1_{Shy}, K^1_{Shy}$ – damping and stiffness coefficients of bearing no. 1 in X, Y direction;

$C^2_{Shx}, K^2_{Shx}, C^2_{Shy}, K^2_{Shy}$ – damping and stiffness coefficients of bearing no. 2 in X, Y direction;

$C^3_{Shx}, K^3_{Shx}, C^3_{Shy}, K^3_{Shy}$ – damping and stiffness coefficients of bearing no. 3 in X, Y direction;

C_V, K_V – damping and stiffness coefficients of the interface between cylinder block and valve port plate;

C_{Hz}, K_{Hz} – damping and stiffness coefficients of the interface between piston and cylinder port;

K_P – stiffness coefficient of the compression spring in separator assembly;

δ_0 – inclination angle of the swash plate;

L_{CF} – distance between points O_C and O_F;

L_{PF} – distance between points O_P and O_F;

L_{F1} – distance between bearing no. 1 and point O_F;

L_{F2} – distance between bearing no. 2 and point O_F;

L_{F3} – distance between bearing no. 3 and point O_F;

L_{F4} – distance between point O_F and mounting plate;

L_{C1} – distance between bearing no. 1 and point O_C;

L_{C2} – distance between bearing no. 2 and point O_C;

L_{C3} – distance between bearing no. 3 and point O_C;

R – radius of the cylinder port circle;

R_V – equivalent radius of force point circle between cylinder block and valve port plate;

L_b – distance between the blind bolt and drive shaft centreline.

The numerical values of parameters were obtained directly by measurements of geometrical quantities of the WPTO2-10 pump (lengths, moments of inertia), estimated experimentally or chosen according to literature data [3, 5]. The table with specification of pump parameters can be found below (Tab. 1).

Table 1.

Specification of pump parameters

Masses and moments of inertia		
Shell set	M_F	12.863 [kg]
	I_{Fx}	614.710 x 10^{-4} [kgm^2]
	I_{Fy}	621.985 x 10^{-4} [kgm^2]

Cylinder block and drive shaft assembly	M_C	2.837 [kg]
	I_{Cx}	106.007 x 10^{-4} [kgm^2]
	I_{Cy}	105.998 x 10^{-4} [kgm^2]
	I_{Cz}	24.950 x 10^{-4} [kgm^2]
Retaining ring	M_P	0.082 [kg]
	$I_{Px'}$	0.246 x 10^{-4} [kgm^2]
	$I_{Py'}$	0.246 x 10^{-4} [kgm^2]
	$I_{Pz'}$	0.437 x 10^{-4} [kgm^2]
Piston shoe	m_S	0.016 [kg]
Piston	m_T	0.048 [kg]
	I_T	0.127 x 10^{-4} [kgm^2]
Stiffness and damping coefficients		
Interface between piston shoe and swash plate	K_{Sw}	Values defined in article
	C_{Sw}	Values defined in article
Interface between cylinder block and valve port plate	K_V	9.80 x 10^9 [N/m]
	C_V	3.60 x 10^7[Ns/m]
Interface between piston and cylinder port	K_{Hz}	1.20 x 10^7[N/m]
	C_{Hz}	3.40 x 10^4[Ns/m]
Bearing no. 1	K^1_{Shx}, K^1_{Shy}	1.60 x 10^9[N/m]
	C^1_{Shx}, C^1_{Shy}	1.00 x 10^7[Ns/m]
Bearing no. 2	K^2_{Shx}, K^2_{Shy}	3.42 x 10^7[N/m]
	C^2_{Shx}, C^2_{Shy}	1.00 x 10^5[Ns/m]
Bearing no. 3	K^3_{Shx}, K^3_{Shy}	4.32 x 10^7[N/m]
	C^3_{Shx}, C^3_{Shy}	2.00 x 10^5[Ns/m]
Separator compression spring	K_P	4.67 x 10^4[N/m]
Bolt between shell and mounting plate	K_{Box}, K_{Boy}	4.00 x 10^7[N/m]
	K_{Boz}	1.00 x 10^8[N/m]
Geometrical quantities		
Distances	L_{CF}	3.5 x 10^{-3}[m]
	L_{PF}	62.0 x 10^{-3}[m]
	L_{F1}	55.5 x 10^{-3}[m]
	L_{F2}	60.5 x 10^{-3}[m]
	L_{F3}	86.7 x 10^{-3}[m]
	L_{F4}	120.0 x 10^{-3}[m]
	L_{C1}	59.0 x 10^{-3}[m]
	L_{C2}	57.0 x 10^{-3}[m]
	L_{C3}	83.2 x 10^{-3}[m]

	L_b	42.5 x 10^{-3}[m]
	R	22.5 x 10^{-3}[m]
	R_V	22.5 x 10^{-3}[m]
	b	30.0 x 10^{-3}[m]
Piston cross-section area	A	1.77 x 10^{-4}[m^2]
Angle of swash plate inclination	δ_0	0.3 [rad]
Suction port pressure	p_0	0.11 [MPa]
Pumping port pressure	p_1	6.60 [MPa]
Pressure fluctuation	Δp	0.60 [MPa]

Assuming small displacements and using kinematic constraints, we can formulate the expressions for kinematic energy, potential energy, dissipation function and generalized forces. Employing Lagrange's equations of the second kind [1, 6] we obtained a system of 13 ordinary, non-homogeneous differential equations of motion with constant coefficients. The equations are juxtaposed below, separately for each assembly of the pump.

Equations for the shell assembly:

$$\begin{aligned}
&M_F\ddot{X}_F + C_{Sw} n \sin\delta_0 \\
&\left\{\left(\dot{Z}_F - \dot{Z}_P\right)\cos\delta_0 + \left(\dot{X}_F - \dot{X}_C\right)\sin\delta_0 + \left(L_{CF} + L_{PF}\right)\dot{\theta}_C \sin\delta_0 - L_{PF}\dot{\theta}_F \sin\delta_0\right\} \\
&+K_{Sw} n \sin\delta_0 \\
&\left\{\left(Z_F - Z_P\right)\cos\delta_0 + \left(X_F - X_C\right)\sin\delta_0 + \left(L_{CF} + L_{PF}\right)\theta_C \sin\delta_0 - L_{PF}\theta_F \sin\delta_0\right\} \\
&\qquad +C^1_{Shx}\left[\left(\dot{X}_F - \dot{\theta}_F L_{F1}\right) - \left(\dot{X}_C - \dot{\theta}_C L_{C1}\right)\right] \\
&\qquad\qquad +C^2_{Shx}\left[\left(\dot{X}_F + \dot{\theta}_F L_{F2}\right) - \left(\dot{X}_C + \dot{\theta}_C L_{C2}\right)\right] \\
&+C^3_{Shx}\left[\left(\dot{X}_F + \dot{\theta}_F L_{F3}\right) - \left(\dot{X}_C + \dot{\theta}_C L_{C3}\right)\right] + K^1_{Shx}\left[\left(X_F - \theta_F L_{F1}\right) - \left(X_C - \theta_C L_{C1}\right)\right] \\
&+K^2_{Shx}\left[\left(X_F + \theta_F L_{F2}\right) - \left(X_C + \theta_C L_{C2}\right)\right] + K^3_{Shx}\left[\left(X_F + \theta_F L_{F3}\right) - \left(X_C + \theta_C L_{C3}\right)\right] \\
&+4K_{Box}\left(X_F + \theta_F L_{F4}\right) = 0
\end{aligned} \tag{1}$$

- -

$$\begin{aligned}
&M_F\ddot{Y}_F + C^1_{Shy}\left[\left(\dot{Y}_F + \dot{\varphi}_F L_{F1}\right) - \left(\dot{Y}_C + \dot{\varphi}_C L_{C1}\right)\right] \\
&+C^2_{Shy}\left[\left(\dot{Y}_F - \dot{\varphi}_F L_{F2}\right) - \left(\dot{Y}_C - \dot{\varphi}_C L_{C2}\right)\right] \\
&\quad +C^3_{Shy}\left[\left(\dot{Y}_F - \dot{\varphi}_F L_{F3}\right) - \left(\dot{Y}_C - \dot{\varphi}_C L_{C3}\right)\right] \\
&\quad +K^1_{Shy}\left[\left(Y_F + \varphi_F L_{F1}\right) - \left(Y_C + \varphi_C L_{C1}\right)\right]
\end{aligned} \tag{2}$$

$$+K_{Shy}^{2}\left[(Y_F-\varphi_F L_{F2})-(Y_C-\varphi_C L_{C2})\right]+K_{Shy}^{3}\left[(Y_F-\varphi_F L_{F3})-(Y_C-\varphi_C L_{C3})\right]$$
$$+4K_{Boy}\left(Y_F-\varphi_F L_{F4}\right)=0$$

$$\begin{aligned}&M_F\ddot{Z}_F+C_{Sw}n\cos\delta_0\left\{\left(\dot{Z}_F-\dot{Z}_P\right)\cos\delta_0+\left(\dot{X}_F-\dot{X}_C\right)\sin\delta_0\right.\\&\left.+\left(L_{CF}+L_{PF}\right)\dot{\theta}_C\sin\delta_0-L_{PF}\dot{\theta}_F\sin\delta_0\right\}\\&+K_{Sw}n\cos\delta_0\left\{\left(Z_F-Z_P\right)\cos\delta_0+\left(X_F-X_C\right)\sin\delta_0\right.\\&\left.+\left(L_{CF}+L_{PF}\right)\theta_C\sin\delta_0-L_{PF}\theta_F\sin\delta_0\right\}\\&+C_V\left(\dot{Z}_F-\dot{Z}_C\right)+K_V\left(Z_F-Z_C\right)+4K_{Boz}Z_F=0\end{aligned}\tag{3}$$

$$\begin{aligned}&I_{Fx}\ddot{\varphi}_F+C_{Sw}R^2\frac{n}{2}\cos\delta_0\left(\dot{\varphi}_F\cos\delta_0-\dot{\varphi}_P\right)+K_{Sw}R^2\frac{n}{2}\cos\delta_0\left(\varphi_F\cos\delta_0-\varphi_P\right)\\&+C_{Shy}^{1}\left[\left(\dot{Y}_F+\dot{\varphi}_F L_{F1}\right)-\left(\dot{Y}_C+\dot{\varphi}_C L_{C1}\right)\right]L_{F1}\\&-C_{Shy}^{2}\left[\left(\dot{Y}_F-\dot{\varphi}_F L_{F2}\right)-\left(\dot{Y}_C-\dot{\varphi}_C L_{C2}\right)\right]L_{F2}\\&-C_{Shy}^{3}\left[\left(\dot{Y}_F-\dot{\varphi}_F L_{F3}\right)-\left(\dot{Y}_C-\dot{\varphi}_C L_{C3}\right)\right]L_{F3}\\&+K_{Shy}^{1}\left[\left(Y_F+\varphi_F L_{F1}\right)-\left(Y_C+\varphi_C L_{C1}\right)\right]L_{F1}\\&-K_{Shy}^{2}\left[\left(Y_F-\varphi_F L_{F2}\right)-\left(Y_C-\varphi_C L_{C2}\right)\right]L_{F2}\\&-K_{Shy}^{3}\left[\left(Y_F-\varphi_F L_{F3}\right)-\left(Y_C-\varphi_C L_{C3}\right)\right]L_{F3}\\&+\frac{1}{2}C_V R_V^2\left(\dot{\varphi}_F-\dot{\varphi}_C\right)+\frac{1}{2}K_V R_V^2\left(\varphi_F-\varphi_C\right)-4K_{Boy}\left(Y_F-\varphi_F L_{F4}\right)L_{F4}\\&+4K_{Boz}L_b^2\varphi_F=0\end{aligned}\tag{4}$$

$$\begin{aligned}&I_{Fy}\ddot{\theta}_F-C_{Sw}L_{PF}n\sin\delta_0\left\{\left(\dot{Z}_F-\dot{Z}_P\right)\cos\delta_0+\left(\dot{X}_F-\dot{X}_C\right)\sin\delta_0\right.\\&\left.+\left(L_{CF}+L_{PF}\right)\dot{\theta}_C\sin\delta_0-L_{PF}\dot{\theta}_F\sin\delta_0\right\}\\&-K_{Sw}L_{PF}n\sin\delta_0\left\{\left(Z_F-Z_P\right)\cos\delta_0+\left(X_F-X_C\right)\sin\delta_0\right.\\&\left.+\left(L_{CF}+L_{PF}\right)\theta_C\sin\delta_0-L_{PF}\theta_F\sin\delta_0\right\}\\&+C_{Sw}\frac{n}{2}\frac{R^2}{\cos^2\delta_0}\left(\dot{\theta}_F-\dot{\theta}_P\right)+K_{Sw}\frac{n}{2}\frac{R^2}{\cos^2\delta_0}\left(\theta_F-\theta_P\right)\\&-C_{Shx}^{1}\left[\left(\dot{X}_F-\dot{\theta}_F L_{F1}\right)-\left(\dot{X}_C-\dot{\theta}_C L_{C1}\right)\right]L_{F1}\\&+C_{Shx}^{2}\left[\left(\dot{X}_F+\dot{\theta}_F L_{F2}\right)-\left(\dot{X}_C+\dot{\theta}_C L_{C2}\right)\right]L_{F2}\end{aligned}\tag{5}$$

$$
\begin{aligned}
&+C^3_{Shx}\left[\left(\dot{X}_F+\dot{\theta}_F L_{F3}\right)-\left(\dot{X}_C+\dot{\theta}_C L_{C3}\right)\right]L_{F3}\\
&-K^1_{Shx}\left[(X_F-\theta_F L_{F1})-(X_C-\theta_C L_{C1})\right]L_{F1}\\
&+K^2_{Shx}\left[(X_F+\theta_F L_{F2})-(X_C+\theta_C L_{C2})\right]L_{F2}\\
&+K^3_{Shx}\left[(X_F+\theta_F L_{F3})-(X_C+\theta_C L_{C3})\right]L_{F3}\\
&+\frac{1}{2}C_V R_V^2\left(\dot{\theta}_F-\dot{\theta}_C\right)+\frac{1}{2}K_V R_V^2\left(\theta_F-\theta_C\right)+4K_{Box}\left(X_F+\theta_F L_{F4}\right)L_{F4}\\
&+4K_{Boz}L_b^2\theta_F=0
\end{aligned}
$$

Equations for the rotor assembly:

$$
\begin{aligned}
&\left[M_C+M_P+n\left(m_T+m_S\right)\right]\ddot{X}_C-\left[M_P\left(L_{CF}+L_{PF}\right)\right.\\
&\left.+n\left(m_T+m_S\right)\left(L_{CF}+L_{PF}\right)-nm_T b\right]\ddot{\theta}_C\\
&-C_{Sw}n\sin\delta_0\left\{\left(\dot{Z}_F-\dot{Z}_P\right)\cos\delta_0+\left(\dot{X}_F-\dot{X}_C\right)\sin\delta_0\right.\\
&\left.+\left(L_{CF}+L_{PF}\right)\dot{\theta}_C\sin\delta_0-L_{PF}\dot{\theta}_F\sin\delta_0\right\}\\
&-K_{Sw}n\sin\delta_0\left\{\left(Z_F-Z_P\right)\cos\delta_0+\left(X_F-X_C\right)\sin\delta_0\right.\\
&\left.+\left(L_{CF}+L_{PF}\right)\theta_C\sin\delta_0-L_{PF}\theta_F\sin\delta_0\right\}\\
&-C^1_{Shx}\left[\left(\dot{X}_F-\dot{\theta}_F L_{F1}\right)-\left(\dot{X}_C-\dot{\theta}_C L_{C1}\right)\right]\\
&-C^2_{Shx}\left[\left(\dot{X}_F+\dot{\theta}_F L_{F2}\right)-\left(\dot{X}_C+\dot{\theta}_C L_{C2}\right)\right]\\
&-C^3_{Shx}\left[\left(\dot{X}_F+\dot{\theta}_F L_{F3}\right)-\left(\dot{X}_C+\dot{\theta}_C L_{C3}\right)\right]-K^1_{Shx}\left[(X_F-\theta_F L_{F1})-(X_C-\theta_C L_{C1})\right]\\
&-K^2_{Shx}\left[(X_F+\theta_F L_{F2})-(X_C+\theta_C L_{C2})\right]-K^3_{Shx}\left[(X_F+\theta_F L_{F3})-(X_C+\theta_C L_{C3})\right]=0
\end{aligned}
\tag{6}
$$

$$
\begin{aligned}
&\left[M_C+M_P+n\left(m_T+m_S\right)\right]\ddot{Y}_C+\left[M_P\left(L_{CF}+L_{PF}\right)+n\left(m_T+m_S\right)\left(L_{CF}+L_{PF}\right)\right.\\
&\left.-nm_T b\right]\ddot{\varphi}_C\\
&-C^1_{Shy}\left[\left(\dot{Y}_F+\dot{\varphi}_F L_{F1}\right)-\left(\dot{Y}_C+\dot{\varphi}_C L_{C1}\right)\right]\\
&-C^2_{Shy}\left[\left(\dot{Y}_F-\dot{\varphi}_F L_{F2}\right)-\left(\dot{Y}_C-\dot{\varphi}_C L_{C2}\right)\right]\\
&-C^3_{Shy}\left[\left(\dot{Y}_F-\dot{\varphi}_F L_{F3}\right)-\left(\dot{Y}_C-\dot{\varphi}_C L_{C3}\right)\right]\\
&-K^1_{Shy}\left[(Y_F+\varphi_F L_{F1})-(Y_C+\varphi_C L_{C1})\right]\\
&-K^2_{Shy}\left[(Y_F-\varphi_F L_{F2})-(Y_C-\varphi_C L_{C2})\right]\\
&-K^3_{Shy}\left[(Y_F-\varphi_F L_{F3})-(Y_C-\varphi_C L_{C3})\right]=0
\end{aligned}
\tag{7}
$$

$$
\begin{aligned}
&M_C\ddot{Z}_C + C_{Hz}n\left(\dot{Z}_C - \dot{Z}_P\right) + K_{Hz}n\left(Z_C - Z_P\right) + C_V\left(\dot{Z}_C - \dot{Z}_F\right) \\
&+K_V\left(Z_C - Z_F\right) + K_P\left(Z_C - Z_P\right) = \sum_{i=1}^{n} F_i(t)
\end{aligned} \tag{8}
$$

$$
\begin{aligned}
&\left\{I_{Cx} + n\left[m_T\left(L_{CF} + L_{PF} - b\right)^2 + m_S\left(L_{CF} + L_{PF}\right)^2 + \frac{1}{2}\left(m_T + m_S\right)R^2\tan^2\delta_0\right]\right. \\
&\left. + M_P\left(L_{CF} + L_{PF}\right)^2 + nI_T\right\}\ddot{\varphi}_C \\
&+\left\{n\left[m_T\left(L_{CF} + L_{PF} - b\right) + m_S\left(L_{CF} + L_{PF}\right)\right] + M_P\left(L_{CF} + L_{PF}\right)\right\}\ddot{Y}_C + I_{Cz}\omega\dot{\theta}_C \\
&-C^1_{Shy}\left[\left(\dot{Y}_F + \dot{\varphi}_F L_{F1}\right) - \left(\dot{Y}_C + \dot{\varphi}_C L_{C1}\right)\right]L_{C1} \\
&+C^2_{Shy}\left[\left(\dot{Y}_F - \dot{\varphi}_F L_{F2}\right) - \left(\dot{Y}_C - \dot{\varphi}_C L_{C2}\right)\right]L_{C2} \\
&+C^3_{Shy}\left[\left(\dot{Y}_F - \dot{\varphi}_F L_{F3}\right) - \left(\dot{Y}_C - \dot{\varphi}_C L_{C3}\right)\right]L_{C3} \\
&-K^1_{Shy}\left[\left(Y_F + \varphi_F L_{F1}\right) - \left(Y_C + \varphi_C L_{C1}\right)\right]L_{C1} \\
&+K^2_{Shy}\left[\left(Y_F - \varphi_F L_{F2}\right) - \left(Y_C - \varphi_C L_{C2}\right)\right]L_{C2} \\
&+K^3_{Shy}\left[\left(Y_F - \varphi_F L_{F3}\right) - \left(Y_C - \varphi_C L_{C3}\right)\right]L_{C3} \\
&+C_{Hz}\frac{n}{2}R^2\left(\dot{\varphi}_C - \frac{\dot{\varphi}_P}{\cos\delta_0}\right) + K_{Hz}\frac{n}{2}R^2\left(\varphi_C - \frac{\varphi_P}{\cos\delta_0}\right) \\
&+\frac{1}{2}C_V R_V^2\left(\dot{\varphi}_C - \dot{\varphi}_F\right) + \frac{1}{2}K_V R_V^2\left(\varphi_C - \varphi_F\right) = R\sum_{i=1}^{n} F_i(t)\cos\alpha_i
\end{aligned} \tag{9}
$$

$$
\begin{aligned}
&\left\{I_{Cy} + n\left[m_T\left(L_{CF} + L_{PF} - b\right)^2 + m_S\left(L_{CF} + L_{PF}\right)^2\right.\right. \\
&\left.\left. + \frac{1}{2}\left(m_T + m_S\right)R^2\left(\tan^2\delta_0 + \tan^4\delta_0\right)\right]\right\}\ddot{\theta}_C \\
&+\left[M_P\left(L_{CF} + L_{PF}\right)^2 + nI_T\right]\ddot{\theta}_C - \left(m_T + m_S\right)\frac{n}{2}R^2\frac{\tan^2\delta_0}{\cos^2\delta_0}\ddot{\theta}_P + \\
&-\left\{n\left[m_T\left(L_{CF} + L_{PF} - b\right) + m_S\left(L_{CF} + L_{PF}\right)\right] + M_P\left(L_{CF} + L_{PF}\right)\right\}\ddot{X}_C - I_{Cz}\omega\dot{\varphi}_C \\
&+C_{Sw}\left(L_{CF} + L_{PF}\right)\sin\delta_0 n\left\{\left(\dot{Z}_F - \dot{Z}_P\right)\cos\delta_0 + \left(\dot{X}_F - \dot{X}_C\right)\sin\delta_0\right. \\
&\left. + \left(L_{CF} + L_{PF}\right)\dot{\theta}_C\sin\delta_0 - L_{PF}\dot{\theta}_F\sin\delta_0\right\}
\end{aligned}
$$

$$
\begin{aligned}
&+K_{Sw}\left(L_{CF}+L_{PF}\right)\sin\delta_0 n\left\{\left(Z_F-Z_P\right)\cos\delta_0+\left(X_F-X_C\right)\sin\delta_0\right.\\
&\left.+\left(L_{CF}+L_{PF}\right)\theta_C\sin\delta_0-L_{PF}\theta_F\sin\delta_0\right\}\\
&+C^1_{Shx}\left[\left(\dot{X}_F-\dot{\theta}_F L_{F1}\right)-\left(\dot{X}_C-\dot{\theta}_C L_{C1}\right)\right]L_{C1}\\
&-C^2_{Shx}\left[\left(\dot{X}_F+\dot{\theta}_F L_{F2}\right)-\left(\dot{X}_C+\dot{\theta}_C L_{C2}\right)\right]L_{C2}\\
&-C^3_{Shx}\left[\left(\dot{X}_F+\dot{\theta}_F L_{F3}\right)-\left(\dot{X}_C+\dot{\theta}_C L_{C3}\right)\right]L_{C3}\\
&+K^1_{Shx}\left[\left(X_F-\theta_F L_{F1}\right)-\left(X_C-\theta_C L_{C1}\right)\right]L_{C1}\\
&-K^2_{Shx}\left[\left(X_F+\theta_F L_{F2}\right)-\left(X_C+\theta_C L_{C2}\right)\right]L_{C2}\\
&-K^3_{Shx}\left[\left(X_F+\theta_F L_{F3}\right)-\left(X_C+\theta_C L_{C3}\right)\right]L_{C3}\\
&+C_{Hz}\frac{n}{2}\frac{R^2}{\cos^4\delta_0}\left(\dot{\theta}_C-\dot{\theta}_P\right)+K_{Hz}\frac{n}{2}\frac{R^2}{\cos^4\delta_0}\left(\theta_C-\theta_P\right)\\
&+\frac{1}{2}C_V R_V^2\left(\dot{\theta}_C-\dot{\theta}_F\right)+\frac{1}{2}K_V R_V^2\left(\theta_C-\theta_F\right)=-\frac{R}{\cos^2\delta_0}\sum_{i=1}^{n}F_i(t)\sin\alpha_i
\end{aligned}
\tag{10}
$$

Equations for the separator assembly:

$$
\begin{aligned}
&\left[M_P+n\left(m_T+m_S\right)\right]\ddot{Z}_P\\
&-C_{Sw}n\cos\delta_0\left\{\left(\dot{Z}_F-\dot{Z}_P\right)\cos\delta_0+\left(\dot{X}_F-\dot{X}_C\right)\sin\delta_0\right.\\
&\left.+\left(L_{CF}+L_{PF}\right)\dot{\theta}_C\sin\delta_0-L_{PF}\dot{\theta}_F\sin\delta_0\right\}\\
&-K_{Sw}n\cos\delta_0\left\{\left(Z_F-Z_P\right)\cos\delta_0+\left(X_F-X_C\right)\sin\delta_0\right.\\
&\left.+\left(L_{CF}+L_{PF}\right)\theta_C\sin\delta_0-L_{PF}\theta_F\sin\delta_0\right\}\\
&+C_{Hz}n\left(\dot{Z}_P-\dot{Z}_C\right)+K_{Hz}n\left(Z_P-Z_C\right)+K_P\left(Z_P-Z_C\right)=-\sum_{i=1}^{n}F_i(t)
\end{aligned}
\tag{11}
$$

$$
\begin{aligned}
&\left[I_{Px'}+\frac{n}{2}\left(m_T+m_S\right)\frac{R^2}{\cos^2\delta_0}\right]\ddot{\varphi}_P+I_{Pz'}\omega\dot{\theta}_P+C_{Sw}\frac{n}{2}R^2\left(\dot{\varphi}_P-\dot{\varphi}_F\cos\delta_0\right)\\
&+K_{Sw}\frac{n}{2}R^2\left(\varphi_P-\varphi_F\cos\delta_0\right)\\
&+C_{Hz}\frac{n}{2}R^2\left(\frac{\dot{\varphi}_P}{\cos^2\delta_0}-\frac{\dot{\varphi}_C}{\cos\delta_0}\right)+K_{Hz}\frac{n}{2}R^2\left(\frac{\varphi_P}{\cos^2\delta_0}-\frac{\varphi_C}{\cos\delta_0}\right)=\\
&-\frac{R}{\cos\delta_0}\sum_{i=1}^{n}F_i(t)\cos\alpha_i
\end{aligned}
\tag{12}
$$

$$\left[I_{Py'} + \frac{n}{2}(m_T + m_S)\frac{R^2}{\cos^4\delta_0}\right]\ddot{\theta}_P - I_{Pz'}\omega\dot{\varphi}_P - \frac{n}{2}(m_T + m_S)R^2\frac{\tan^2\delta_0}{\cos^2\delta_0}\ddot{\theta}_C$$

$$+C_{Sw}\frac{n}{2}\frac{R^2}{\cos^2\delta_0}\left(\dot{\theta}_P - \dot{\theta}_F\right) + K_{Sw}\frac{n}{2}\frac{R^2}{\cos^2\delta_0}(\theta_P - \theta_F) \tag{13}$$

$$+C_{Hz}\frac{n}{2}\frac{R^2}{\cos^4\delta_0}\left(\dot{\theta}_P - \dot{\theta}_C\right) + K_{Hz}\frac{n}{2}\frac{R^2}{\cos^4\delta_0}(\theta_P - \theta_C) = \frac{R}{\cos^2\delta_0}\sum_{i=1}^{n}F_i(t)\sin\alpha_i$$

In the above equations of motion (1–13), there are the following additional symbols:

b – half length of piston;

n – number of pistons in cylinder block ($n = 7$);

$\alpha_i = \omega t + (i-1)\dfrac{2\pi}{n}$ – angular displacement of i-th piston (Fig. 3b);

$F_i(t) = p_i(t) \cdot A$ – instantaneous force in i-th cylinder port, where:

ω – constant angular velocity of drive shaft ($\omega = 157$ [rad/s]);

A – piston cross-section area;

$p_i(t)$ – pressure course in i-th cylinder port (Fig. 4).

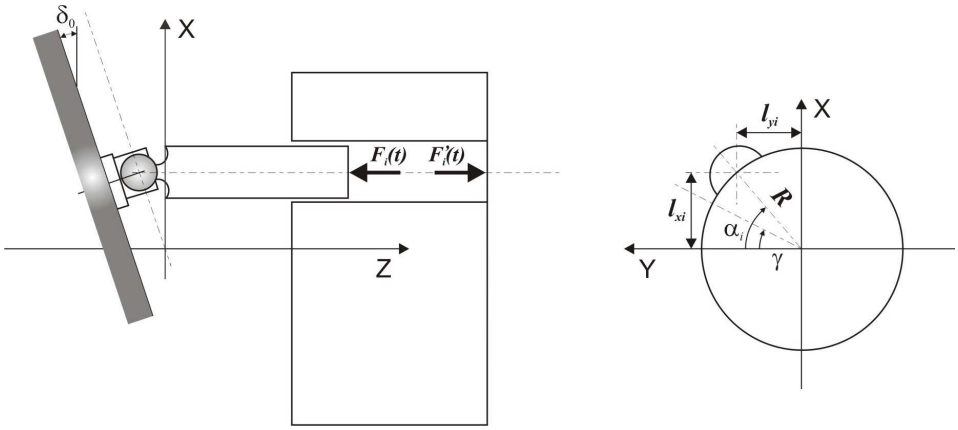

Fig. 3b. Geometrical relations referring to instantaneous force in i-th cylinder port

The above equations of motion can be written down in a vector form:

$$[M]\{\ddot{q}\} + [C]\{\dot{q}\} + [K]\{q\} = \{Q(t)\} \tag{14}$$

where:

$\{q\} = \{X_F, Y_F, Z_F, \varphi_F, \theta_F, X_C, Y_C, Z_C, \varphi_C, \theta_C, Z_P, \varphi_P, \theta_P\}$ – vector of generalized coordinates;

$[M]$ – mass matrix;

$[C]$ – damping matrix;
$[K]$ – stiffness matrix;
$\{Q(t)\}$ – vector of generalized forces.

To obtain a solution and perform simulation investigation on the dynamics of pump model described by the vector equation (**??**), we had to create a dedicated computer program, written in C language. The program makes use of the Fourier series and superposition method and allows for:

- registering the courses of vibration accelerations at a selected point of the pump body;
- simulating the influence of changes of chosen model parameters (for example: stiffness coefficients, damping coefficients, working pressure) on the registered courses of vibration accelerations;
- plotting phase trajectories for selected points of the body pump.

Additionally, the program makes it possible to determine courses of vibrations in the pump model in relationship with the shape of the assumed time-function of pressure in the cylinder port.

The graphs in Fig. 4 illustrate the theoretical course of pressure in the cylinder port (a) and the approximation of this course used in our simulation investigations (b).

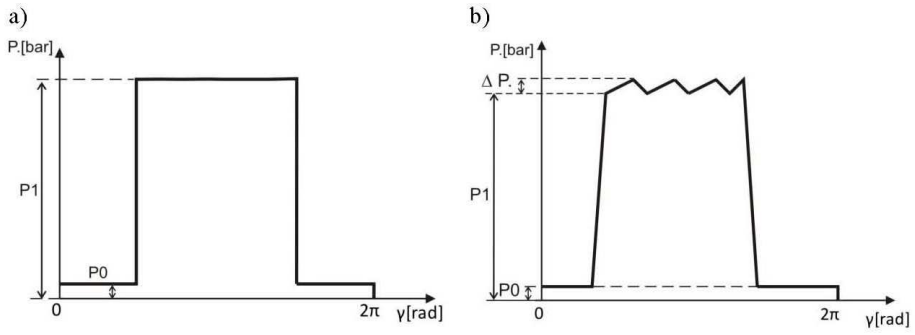

Fig. 4. Assumed cylinder port pressure courses for the working cycle of pump: a) theoretical course b) approximation of the real course

4. Initial simulation research on the developed model

According to the authors' intention, the developed dynamic model of the multi-piston pump should be used for damage simulation in its individual elements. By gradual change in values of selected construction parameters of the object (for example: stiffness coefficients, damping coefficients), it is possible to perform simulation of wear in the pump. Initial verification of performance of the created model was done to examine the effect of abrasive

wear on the swash plate surface. The role that the swash plate plays in the construction (Fig. 5) is, among other things, to guarantee proper setting of the pump's efficiency by changing the inclination angle of the swash plate, which affects the length of stroke of the piston in the rotor cylinder and influences the volume of the pumped medium in the working cycle of a pump.

Physically, the swash plate cooperates with the surfaces of piston shoes, which while performing the rotational motion, slide on its surface. In this action, there occur losses which result from abrasion on surfaces of cooperating elements. A reduction in losses, and in consequence – an increase in the mechanical and hydraulic efficiency of the whole device, is obtained through hydrostatic propping of the shoes on the plate surface. In the case when such a propping disappears, there occurs progressive wear of the plate surface (and the piston shoes) which leads to the creation of an elliptic pit on its surface and its total wear (Fig. 5).

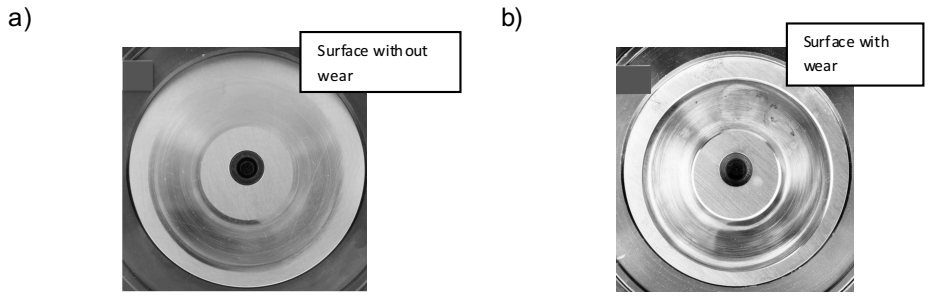

Fig. 5. View of the swash plate surface condition:

a) functional plate – without wear b) surface of worn-out plate

In the developed model, the cooperation between the swash plate surface and the surfaces of the piston shoes of the rotor assembly was described by means of adequately chosen values of stiffness coefficient K_{Sw} and damping coefficient C_{Sw}. Based on literature review [4] and experimental research conducted by the authors, it was found that disappearance of the lubricating layer (which speeds up the process of abrasive wear of the plate surface) leads to an increase in damping and to an increase in stiffness between the cooperating elements. By properly increasing the values of damping and stiffness coefficients assumed in the simulation investigation, it was possible to model the changes in work conditions of the pump which led to the damage of the swash plate.

Usually, in the case of a real pump, diagnostic information is obtained by registering vibration from measurement transducers installed at specific

places on the pump body. Similarly, in the created model, we envisaged the possibility of registering vibration components in the directions X, Y, and Z at any place on the pump body. In the case of simulation investigation on the swash plate wear, vibration accelerations were calculated for the places on the shell which were directly adjacent to the examined element (measurement points P1, P4 and P7) and additionally for the rotors (measurement points P2 and P5) and for the control plate (measurement points P3 and P6). The allocation of measurement points on the pump model is presented in Fig 6.

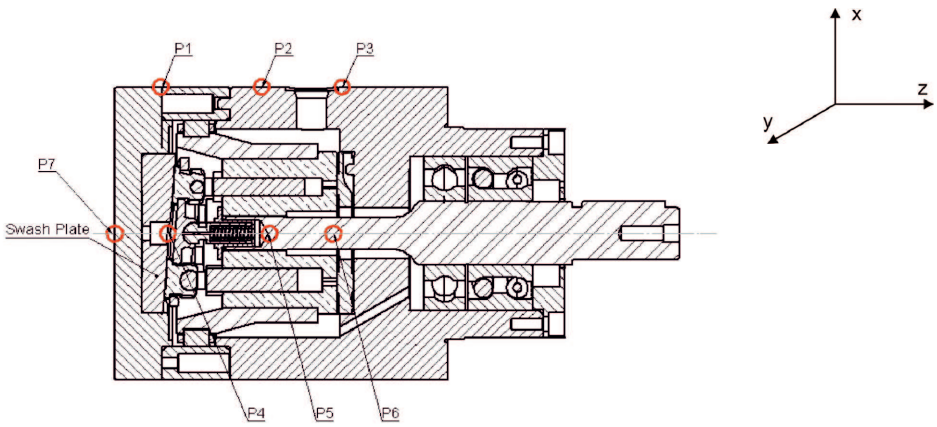

Fig. 6. Distribution of measurement points on the pump body in model testing

Fig. 7 illustrates sample courses of vibration acceleration obtained at the assumed points of the pump body model (points P1, P4 and P7) for chosen values of damping and stiffness coefficients: C_{Sw}=1.86×10^6 [Ns/m], K_{Sw}=4.3×10^7 [N/m]. With such coefficients values, there exist conditions of hydrostatic propping of shoes on the plate surface (no abrasive wear). We also assumed the real shape of pressure course in the cylinder ports of the rotor (Fig. 4b).

Apart from vibration accelerations calculated at the chosen points of the object, the developed computer program also allows for calculating components of displacement and velocity needed to determine phase trajectories. By tracing the changes of phase trajectory courses, one can often easily estimate wear in the investigated object. The phase space contains information about the accumulated energy (the sum of kinetic and potential energy) of the examined object. The change of this energy is represented in the phase space by the change in the shape of trajectory, and the area it encompasses. The plots below represent phase trajectories determined at chosen measurement

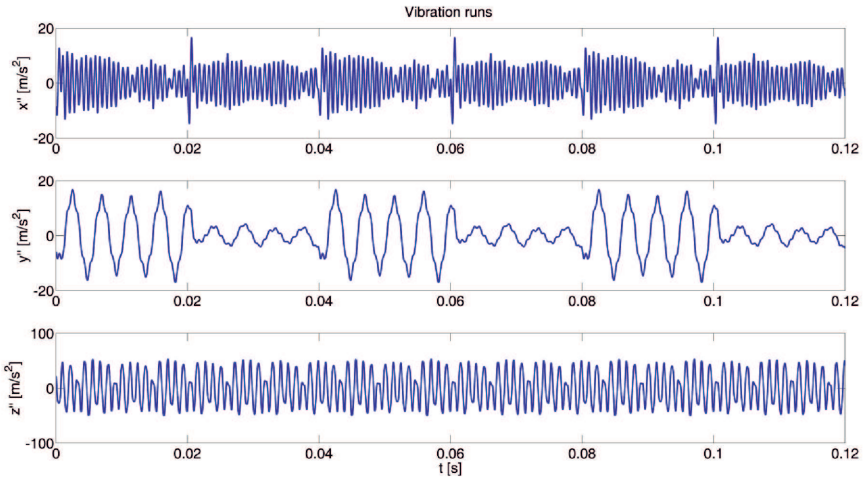

Fig. 7. Example of vibration courses at point P1, P4 and P7 of the pump model

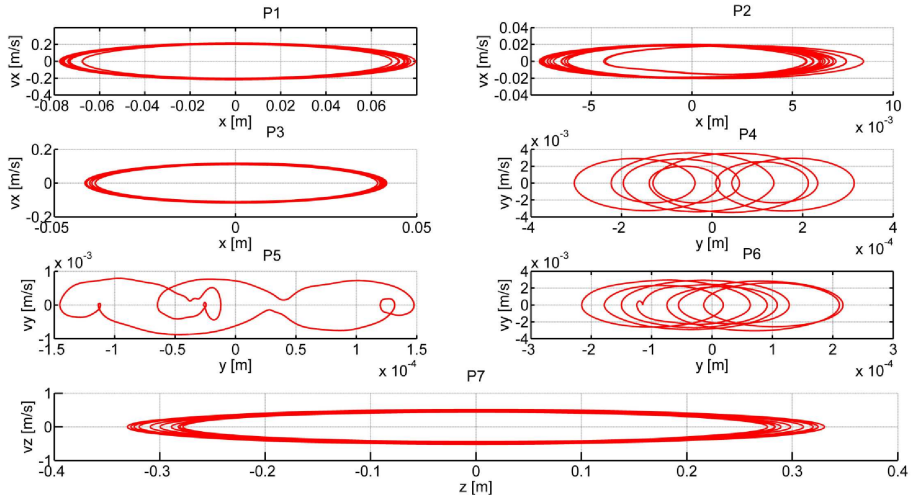

Fig. 8. Phase trajectory plots determined at the chosen points on pump casing for the theoretical pressure course (Fig. 4a) in cylinder port

points (shown in Fig. 5) for the theoretical (Fig. 8) and real pressure courses in the cylinder port (Fig. 9).

The preliminary simulation investigation were aimed, among other things, at verifying the correctness of the created dynamic model of the pump and consisted in determining phase trajectories at previously assumed measurement points (Fig. 5). By gradually increasing the values of parameters C_{Sw} and K_{Sw}, we modelled the effect of limiting the hydrostatic propping of

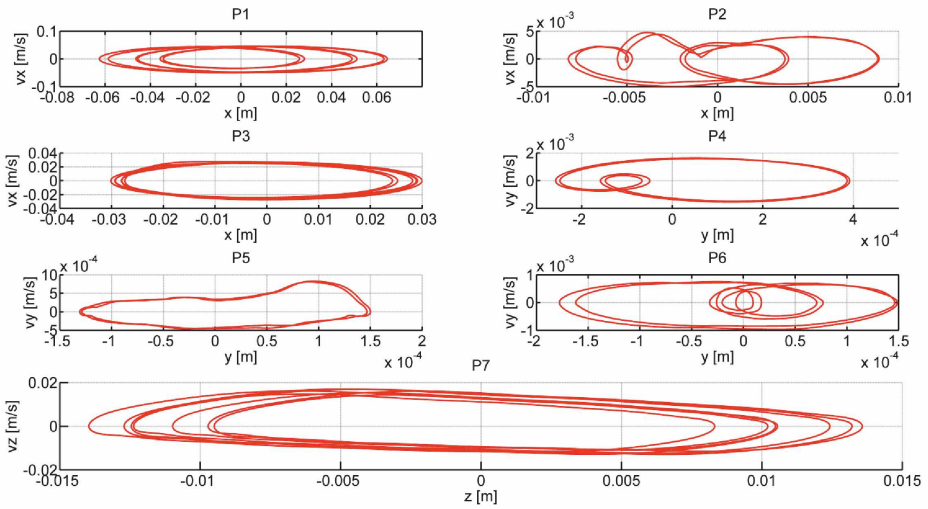

Fig. 9. Phase trajectory plots determined at the chosen points on pump casing for the real pressure course (Fig. 4b) in cylinder port

piston shoes on the swash plate surface, until it completely vanished (the process of abrasive wear occurred). The simulation was conducted for the pump working with static pressure of 7 [MPa] (Fig. 4), under the assumption of the real pressure course in the cylinder port (Fig. 4b).

Juxtaposition of example phase trajectories obtained for the assumed initial values of damping and stiffness coefficients C_{Sw}, K_{Sw} of the interface between piston shoe and swash plate for the directions X (point P1), Y (point P4) and Z (point P7) is presented in Figs. 10-12.

Additionally, the arrows mark directions of phase trajectory changes resulting from an increase in values of the parameters C_{Sw} and K_{Sw}.

5. Summary and final conclusions

On the basis of the conducted simulation investigation, we can state that it is possible to estimate limit values of damping coefficient C_{Sw} and stiffness coefficient K_{Sw} at which the lubricating layer disappears, and abrasive wear appears in cooperating pump elements. Further increase in the values of C_{Sw} and K_{Sw} does not substantially influence neither the shape of the received vibration acceleration course, nor the phase trajectories. Then, there exists a limit trajectory, beyond which the examined device undergoes an abrupt process of wear (for example, dry abrasion occurs). Providing that a quantitative measure for such a trajectory is found, we might expect obtaining a valuable diagnostic information about the state of wear in pump elements.

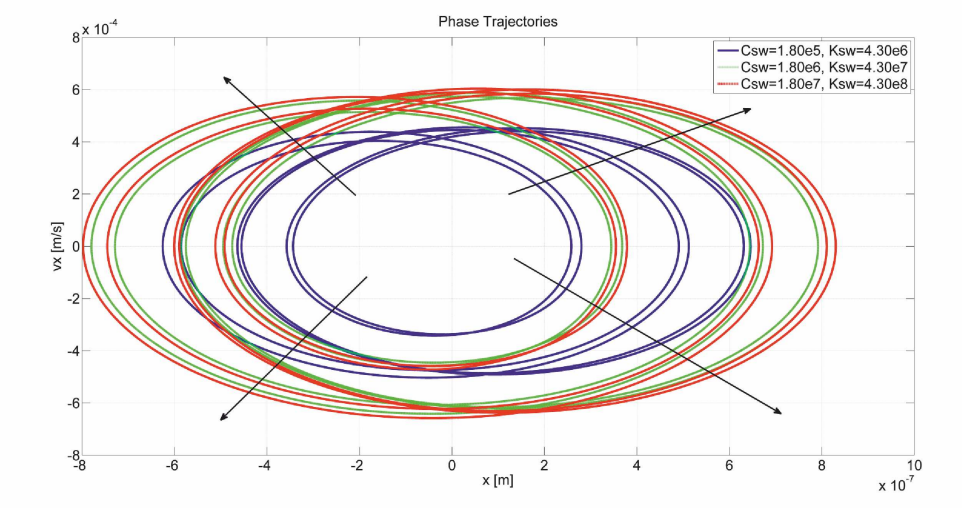

Fig. 10. Comparison of phase trajectories obtained at point P1 of the pump model (in X direction)

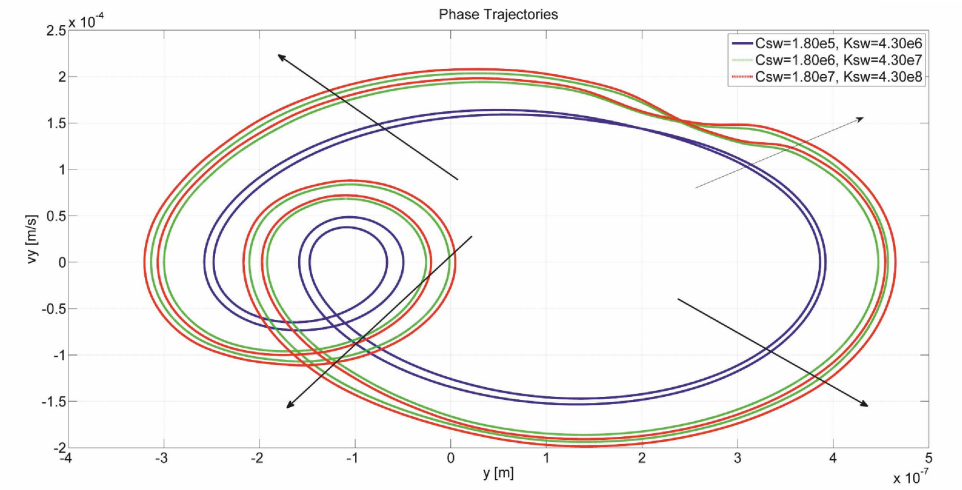

Fig. 11. Comparison of phase trajectories obtained at point P4 of the pump model (in Y direction)

The initial verification of the created dynamic model of the axial piston pump confirmed its functionality. The conducted simulation investigation allows us to state that the developed model works properly. The calculated vibration accelerations are qualitatively consistent with the changes in selected physical parameters of the model.

The presented phase trajectories determined at chosen points of the body may constitute an additional non- parametrical measure of the efficiency state of the pump. Further research on the model will be aimed at reaching better consistency between the obtained results of simulation and the results of

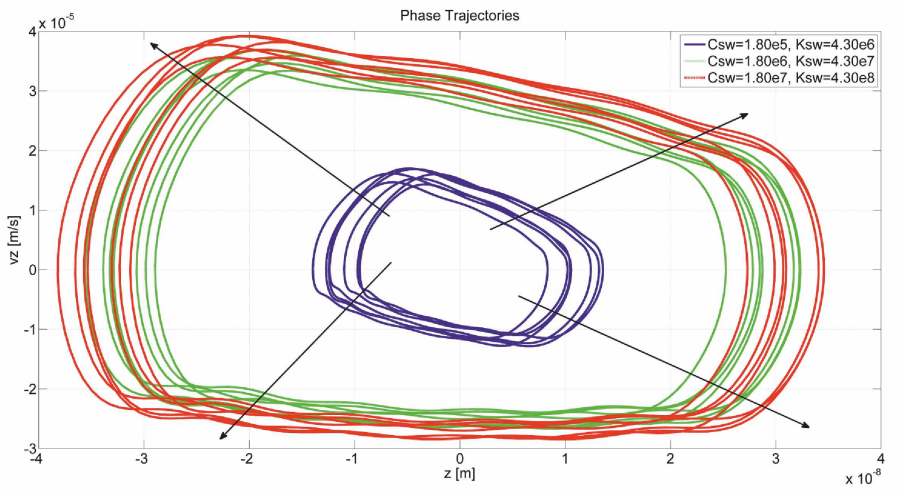

Fig. 12. Comparison of phase trajectories obtained at point P7 of the pump model (in Z direction)

measurements on a real pump object realized through identification of the pump's coefficient values.

Research carried out within the confidences of KBN grant no. N501325135

Manuscript received by Editorial Board, November 18, 2010;
final version, April 14, 2011.

REFERENCES

[1] Adams M.: Rotating Machinery Vibration. CRC Press Inc., 2010.
[2] Bogusz W.: Technical stability. PWN, Warsaw 1972 (in Polish).
[3] Chen H. X., Patrick S. K. Chua and Lim G. H.: Dynamic vibration analysis of a swash-plate type water hydraulic motor. Mechanism and Machine Theory, Volume 41, Issue 5, May 2006, Pages 487-504.
[4] Edge K. A., Darling J.: The pumping dynamics of swash plate piston pumps. Journal of Dynamic Systems, Measurement and Control, Trans. of ASME, No 111, 1989.
[5] Nishimura T., Umeda T., Tsuta T., Fujimara M., Kamakami M.: Dynamic response analysis of a swash-plate type hydraulic piston pump. ASME, 1995, Pages 145-155.
[6] Josephs H., Huston R. L.: Dynamics of Mechanical Systems. CRC Press Inc., 2002.
[7] Stryczek S.: Hydraulic Drive. WNT, Warsaw 1995 (in Polish).
[8] Vacca A., Klop R., Ivantysynova M.: A numerical approach for the evaluation of effects of air release and vapour cavitation on effective flow rate of axial piston machines. International Journal of Fluid Power, No 1, 2010, Pages 33-45.
[9] Żółtowski B., Cempel C.: Engineering of Machines Diagnosis. PTDT Press, Radom 2004 (in Polish).
[10] Basic Principles and Components. The Hydraulic Trainer, Vol. 1 Hydraulic – Rexroth Bosch Group.
[11] http://www.pzl-wroclaw.com.pl/

Model dynamiczny pompy tłokowej w diagnostyce zużycia jej elementów składowych

S t r e s z c z e n i e

Możliwość rozróżnienia i oceny wpływu poszczególnych uszkodzeń elementów pompy w rejestrowanym przebiegu drgań jej korpusu stanowiłoby cenne źródło informacji diagnostycznej. Efektywnym narzędziem do osiągnięcia tego celu może być dobrze zaprojektowany i zidentyfikowany model dynamiczny, który zastosowany do konkretnego typu pompy mógłby dodatkowo pomóc w ulepszeniu jej konstrukcji.

W prezentowanym artykule przedstawiono opracowany model dynamiczny osiowej pompy tłokowej. Przyjęte założenia upraszczające wraz z dokonanym podziałem pompy na zespoły pozwoliły na opis jej działania modelem dyskretnym o 13-stu stopniach swobody.

Zbudowany model dynamiczny pompy – w założeniach autorów – posłużyć ma do symulacji uszkodzeń jej poszczególnych elementów. Poprzez stopniową zmianę wartości wybranych parametrów konstrukcyjnych pompy (np. współczynników sztywności, tłumienia) możliwa jest symulacja rozwoju zużycia całej pompy, jak i poszczególnych jej elementów.

W pracy przedstawiono wstępną weryfikację poprawności działania opracowanego modelu na przykładzie symulacji zużycia ściernego powierzchni tarczy wychylnej. Jako źródło informacji diagnostycznej o stanie zużycia elementu składowego wykorzystano przebiegi trajektorii fazowych w punktach charakterystycznych korpusu pompy.